

A Two-Level Approach for Design Optimization of Acoustic Liners

Emre Özkaya¹, Junis Abdel Hay¹, Nicolas R. Gauger¹, Norbert Schönwald², Frank Thiele²

¹ Chair for Scientific Computing, TU Kaiserslautern, 67663 Kaiserslautern, Germany

² CFD Software Entwicklungs- und Forschungsgesellschaft mbH, 14163, Berlin, Germany

Corresponding author: emre.oezkaya@scicomp.uni-kl.de

Abstract: In this paper, we present a novel two-level approach for design optimization of acoustic liner panels that are commonly used to damp engine noise in turbofan engines. The method combines an adjoint-based gradient search algorithm with a global search method applied on a surrogate model. In this way, we effectively exploit the benefits of both approaches to achieve a good compromise between computational effort and degree of freedom used in optimization. In the first level, a global search is performed with few design parameters employing a Gaussian process surrogate model. In the second level, taking the global optimal solution as the initial setting for the refined design vector, an adjoint based gradient search procedure is started. The unsteady discrete adjoint solver, which is an essential ingredient of the optimization framework, has been developed using Algorithmic Differentiation (AD) techniques. The AD generates a robust discrete adjoint solver, which solves the unsteady adjoint Linearized Euler Equations (LEE) backward-in-time. The feasibility of the two-level approach is demonstrated by finding the optimal liner parameters of a turbofan engine by-pass duct.

Keywords: Computational Aeroacoustics, Numerical Optimization, Engine Noise Reduction.

1 Introduction

The noise pollution caused by increasing air traffic has been a serious environmental problem in residential areas, which are close to big airports. Therefore, reducing the aircraft noise has been an important goal in various national or supranational research activities, e.g. Horizon 2020 program initiated by the European Union. Especially during take-off of airplanes, engine noise is the most significant sources of noise emission. Therefore, damping the engine noise is crucial in reducing the overall noise emission of an aircraft. In modern turbofan engine design, passive noise damping of the engine noise through installation of acoustic liner panels is a well established technique. These panels typically consist of a perforated top layer, called face-sheet, and a honeycomb structure placed on top of a rigid back-sheet. During manufacturing process, these liner panels are usually installed on the internal walls of the engine nacelle, both in the engine intake and in the by-pass duct. Thanks to the recent achievements in acoustic impedance modeling, nowadays it has become feasible to simulate the effect of acoustic liners on the engine noise in a Computational Aeroacoustics (CAA) framework. As a result, it has become viable to make a rapid assessment of different possible liner configurations by performing CAA simulations.

One crucial issue in the design of acoustic liners is the specification of liner parameters. To date, it is common to specify the liner parameters either based on experimental knowledge or by performing trial-and-error type of CAA simulations. However in recent years, it has become tempting to use numerical design optimization studies to determine liner parameters. If the number of design parameters in these

studies is only a few, gradient-free optimization methods can be applied. By increasing number of design parameters, however, employing gradient-based algorithms coupled with an adjoint solver becomes more and more attractive. In fact, if the dimension of the design vector is large, using adjoint solvers to evaluate the gradient vector becomes essential since they can evaluate the gradient vectors at a fixed computational effort. Therefore, optimization studies with a high degree of freedom become viable. Broadly speaking, the adjoint approaches can be classified into two: continuous and discrete adjoint methods. In the continuous adjoint method [1], one first derives the optimality conditions from the continuous optimization problem. The resulting adjoint PDE is then discretised by using appropriate spatial and temporal schemes, and solved using standard numerical methods. In general, continuous adjoint solvers are fast in run-time, but development of them requires much effort. Furthermore, the maintenance of these solvers becomes a burden as the underlying PDE solvers are subject to continuous modifications, e.g., new boundary conditions, new physical models etc. As an alternative, using the discrete adjoint method, one derives the discrete adjoint equation directly from the optimization problem written using the discretized state PDE. In general, developing discrete adjoint solvers is more straightforward. Therefore, discrete adjoint codes have found a wider acceptance in CFD, especially for the large scale applications with complex geometries.

The discrete adjoint PDE solvers can be developed either by hand [2] or by using the Algorithmic Differentiation (AD) techniques [3]. Using the so-called hand-discrete approach, one derives first the discrete adjoint equation for the given objective function. In the derivation, the linearization of discrete residuals is often performed using symbolic differentiation rules. A computer program is then written to implement to solution scheme for the adjoint equation and to evaluate the gradient vector. Although the hand-discrete approach usually leads to efficient adjoint solvers, the implementation is error-prone as the linearization is performed by hand. Furthermore, similar to continuous adjoint solvers, any modifications in the objective function or in the underlying state PDE solver result in reformulation and recoding in the adjoint part.

As an alternative to the hand-discrete approach, AD tools can be used to automatically generate discrete adjoint solvers. In this way, the exact differentiation of the underlying PDE solver can be done without much effort. Since all terms in the discrete residual can be differentiated exactly, adjoint codes generated by AD tools are capable of computing sensitivities that are always accurate and consistent to the solutions of the state PDE. Furthermore, the adjoint solver inherits robustness of the underlying PDE solver and does not require special treatment, e.g., extra grid refinement, special tuning of solver parameters etc. Thanks to these positive aspects, AD techniques have been successfully applied in developing discrete adjoint solvers in the past for CFD and CAA applications [4, 5].

Although being computationally very efficient, in some cases, adjoint-based gradient search methods may perform poorly since these algorithms tend to be trapped to local optima. In problems, in which the response surface is fairly noisy, typically the optimization method stagnates after yielding some moderate improvement within few cycles. In addition, gradient-based algorithms are usually very sensitive to the initial value of the design vector. Therefore, a "bad" choice for the initial value, which is far from the global optimum, may result in a poor performance. As a remedy to this problem, a global optimization methods can be employed. For example, Evolutionary Algorithms (EAs) [6, 7], which try to imitate the evolution process in the nature, are widely applied for design optimization problems. These algorithms, however, are computationally expensive and they require a prohibitive amount of computational resources if the number of design parameters is large. For this reason, in general, EAs are only applicable to limited problems with few design variables. In many cases, they are applied not directly to the full scale simulation but in conjunction with surrogate modeling techniques such as radial basis functions or Kriging method [8, 9, 10].

In the present work, we suggest an efficient two-level design strategy that combines an EA based global optimization using a surrogate model and a gradient-based optimization using a discrete adjoint solver generated by AD techniques. In this way, we benefit from both approaches, and try to achieve a good compromise between computational effort and fidelity of the optimization. In the first level, a global search is performed with few design parameters used to parameterize the liner. The surrogate model required for the EA is build using a Gaussian process surrogate model. In the second level, taking the global optimal solution as the initial setting for the refined liner parameterization, an adjoint based gradient search procedure is started.

A similar optimization strategy for the aerodynamic shape optimization is suggested by Yim et al. [11].

This paper is organized as follows. In Section 2, the governing equations, the CAA solver and the acoustic impedance modeling used in this work is introduced. In Section 3, we present the two-level optimization approach. In Section 4, we introduce the annular by-pass duct configuration of fan test rig, which is used as the test case to demonstrate the efficiency of suggested two-level approach. We also present the optimization results, which are obtained by the liner optimization. Finally, we draw some conclusions in Section 5.

2 CAA Framework

In this section, we introduce the CAA framework used to simulate the sound propagation in the present work. First the governing equations are briefly introduced. Then, we shortly mention the features of the CAA solver and the acoustic impedance modeling used to model the damping of the liner.

2.1 Governing Equations

Since run-time requirements of full CFD simulations are too high for applications of practical relevance, hybrid or zonal approaches are rather used to simulate the aeroacoustic phenomena. In these approaches, typically the domain of interest is split into three different zones: the source zone, the propagation zone and the far-field zone. Thanks to this splitting, different physical phenomena in each zone can be simulated using optimized numerical methods and the computational effort can be significantly reduced. Inside the source zone, there are several noise generation mechanisms present in the flow such as rotor-stator interactions or perturbations occurring in the combustion chamber. These noise sources, either broadband or tonal, are in general resolved using high fidelity CFD simulations. The propagation zone, on the other hand, is free of acoustic sources so that the acoustic waves propagate inside the engine interacting with hard walls and liner panels. In the far-field zone, the acoustic waves propagate in the surrounding medium until they are totally dissipated. In the present work, we only focus on the propagation zone. In this region, the Linearized Euler Equations (LEE) are appropriate to simulate the aeroacoustic wave propagation. The LEE equations, which are derived from the Euler equations, are given in tensor notation as

$$\begin{aligned} \frac{\partial \rho'}{\partial t} + \bar{u}_i \frac{\partial \rho'}{\partial x_i} + u'_i \frac{\partial \bar{\rho}}{\partial x_i} + \bar{\rho} \frac{\partial u'_i}{\partial x_i} + \rho' \frac{\partial \bar{u}_i}{\partial x_i} &= 0, \\ \frac{\partial u'_i}{\partial t} + \bar{u}_j \frac{\partial u'_i}{\partial x_j} + u'_j \frac{\partial \bar{u}_i}{\partial x_j} + \frac{\rho'}{\bar{\rho}} \bar{u}_j \frac{\partial \bar{u}_i}{\partial x_j} + \frac{1}{\bar{\rho}} \frac{\partial p'}{\partial x_i} &= 0, \\ \frac{\partial p'}{\partial t} + \bar{u}_i \frac{\partial p'}{\partial x_i} + u'_i \frac{\partial \bar{p}}{\partial x_i} + \gamma \bar{p} \frac{\partial u'_i}{\partial x_i} + \gamma p' \frac{\partial \bar{u}_i}{\partial x_i} &= 0. \end{aligned}$$

In the LEE equations, u'_i is the oscillating part of the velocity component u_i , p' is the oscillating part of the pressure, ρ' is the oscillating part of density, \bar{u}_i is the mean velocity component, \bar{p} is the mean pressure, $\bar{\rho}$ is the mean density and γ is the ratio of specific heats. Compared to the Navier-Stokes simulations, in which very fine grids are required, LEE simulations are much cheaper in terms of computational resources as optimized spatial and temporal schemes tailored for CAA can be used.

2.2 CAA Solver

In the present work, we use the 3D finite difference code CAA code *CFD-Noise* of CFD Software Entwicklungs- und Forschungsgesellschaft mbH Berlin to solve the LEE equations. The spatial scheme is the 7-point 4th order Dispersion-Relation-Preserving (DRP) scheme developed by Tam & Webb [12]. The forward-in-time integration is achieved by using the Low-Dissipation and Low-Dispersion Runge-Kutta (LDDRK) scheme of Hu et al. [13], using the $2N$ storage form proposed by Stanescu et al. [14]. The boundary conditions include hard walls and non-reflective boundary conditions such as the radiation boundary condition by Tam [15] and Perfectly Matched Layer (PML) boundary condition proposed by Hu [16]. In order to eliminate the parasitic short-wave components, a tenth-order low-pass filter is applied. Moreover, the Chimera grid capability enables the CAA solver to handle with complex geometries.

2.3 Acoustic Impedance Modeling using Extended Helmholtz Resonator Model

As far as the modeling of the liner is concerned, we use the Extended Helmholtz Resonator (EHR) model suggested by Rienstra [17]. The EHR model was introduced as a high frequency extension of the classical Helmholtz Resonator model and describes the impedance of a damped Helmholtz resonator. It is given in frequency domain as

$$Z(i\omega) = R_f + i\omega m_f - i\beta \cot\left(\frac{1}{2}\omega T_l - i\frac{1}{2}\epsilon\right). \quad (1)$$

In the above equation $Z(i\omega)$ is the acoustic impedance and it is defined as the ratio between the complex amplitudes of pressure \hat{p} and the velocity perturbation \hat{u}_n in the normal direction, i.e., $Z(i\omega) = \hat{p}(i\omega)/\hat{u}_n(i\omega)$. The five model parameters $R_f, m_f, \epsilon, \beta$ and T_l used in Eq. 1 are positive real numbers. According to Rienstra, R_f and m_f correspond the resistance and reactance of the liner face sheet. Furthermore, compared to the classical Helmholtz resonator model, the three modifications had been incorporated to the EHR model. First, the parameter ϵ accounts for the dissipation due to damping in the fluid cavity. Second, the cotangent term is scaled by the parameter β to obtain a varying cavity reactance. Finally, the time delay parameter T_l is included in the model to account for the cavity depth.

The representation of the EHR model in the time domain is achieved by z -transformation, which is also suggested by Rienstra [17]. The effect of the grazing flow is modeled by the Ingard/Myers boundary condition [18, 19]. In time-domain, EHR model leads to a boundary condition in terms of velocity perturbation in the normal direction:

$$\begin{aligned} \frac{\partial u'_n}{\partial t}(t) &= \frac{1}{m_f} [\mu(t) - (R_f + \beta)u'_n(t)] \\ &- \frac{e^{-\epsilon}}{m_f} [\mu(t - T_l) - (R_f - \beta)u'_n(t - T_l)] + e^{-\epsilon} \frac{\partial u'_n}{\partial t}(t - T_l), \end{aligned} \quad (2)$$

where $\mu(t)$ is given by

$$\mu(t) = p' + \mathbf{u}_0 \cdot \nabla p' - \mathbf{n} \cdot (\mathbf{n} \cdot \nabla \mathbf{u}_0) p'.$$

In the present work, we take a parameterization such that the entire liner surface can be split into a number of different patches. In this setting, the parameters of the EHR model are only allowed to vary among the different liner patches. The number of patches taken for the optimization, on the other hand, is specified by the user and thus can be arbitrarily large.

3 The Two-Level Approach

Since gradient-based optimization results are highly sensitive to the initial values, the initial setting for the design parameters plays a crucial role in the success of optimization. In numerical design optimization of acoustic liners, one can use values obtained from previous simulations and/or experimental results to initialize the liner parameters at the beginning of optimization. However, these values are likely to be far away from the global optimum and the reduction of the objective function achieved by the numerical optimization may not be satisfactory. On the other hand, if only a single liner patch is used, the design vector has only five parameters and applying an EA based optimization using a surrogate model becomes viable. In this way, a better initial setting for the gradient-based optimization can be achieved. In the initial data acquisition phase, which is required to train the surrogate model, first CAA simulations at a number of specified sample design points are performed. Once the initial data set is available, a surrogate model is constructed. Note that, at this stage the surrogate model approximates the true response surface only up to some accuracy. Using the surrogate model, then a global search based on EA is started. Since evaluating performance of new designs using the surrogate model is computationally much cheaper compared to CAA simulations, the number of samples in the global search can be taken much larger than the number of samples taken for the initial data acquisition. Once the "best" initial setting for the liner parameters is found, the number of liner patches can be increased to enhance the fidelity of the optimization. At this second stage, using a gradient-based optimization method coupled with an adjoint solver is appropriate. In Figure 1, the two-level

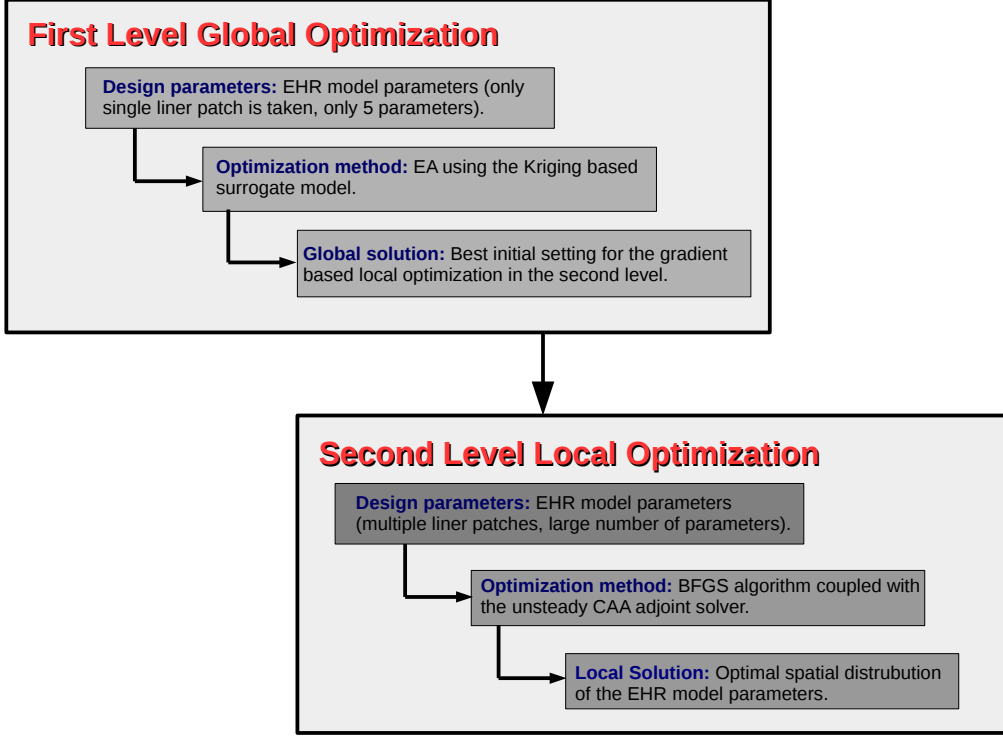


Figure 1: Schematic illustration of the two-level approach

approach is illustrated schematically.

In the following, we first introduce the global optimization strategy used in the first level. Thereby, we give a special emphasis on the surrogate model since the quality of it plays a key role in the success of the global search. Then, we introduce the discrete adjoint methodology used to develop the discrete adjoint CAA solver, which is used to evaluate the gradient vector in the gradient search in the second level.

3.1 Global Search Based on a Surrogate Model

Since CAA simulations, required to calculate the value of the objective function for a given liner design, are computationally very expensive, we suggest to use a surrogate model. In the present work, the surrogate model is constructed using the Kriging method, which is introduced briefly in following.

The Kriging method [20] (also called as the DACE stochastic process model [21]) is an interpolating method, which features the function to be interpolated at all sample points. It provides a statistic prediction of an unknown function by maximizing the likelihood of the estimate. The Kriging method can cope with unevenly distributed data, and therefore it is well suited for the problems with highly-nonlinear response surfaces having multiple extrema. For the derivation of Kriging, the output data obtained from n_s different deterministic computer simulations $Y_i = f(X_i)$, $i = 1, \dots, n_s$ is treated as a realization of a stochastic process, which is defined as the sum of a global trend function and an error term

$$\tilde{f}(X, \beta) = g^\top(X)\beta + Z(X)$$

The key assumption made while deriving the Kriging estimator is that the error term $Z(X)$ is a Gaussian process. In the present work, we adopt the so-called ordinary Kriging approach, in which the trend function is assumed to be constant, i.e., $g^\top(X)\beta = \beta_0$. Note that, due to the Gaussian process assumption, the Kriging estimator interpolates the function f at the sample points with zero uncertainty, i.e., $\tilde{f}(X_i, \beta_0) = Y_i$, $i =$

$1, \dots, n_p$. We tacitly assume that sample points are exact, i.e., the errors due to modeling and discretization errors in the simulations are neglected. Furthermore, $Z(X)$ is assumed to be a stationary random process with a zero mean, positive variance and covariance. The correlation function between two arbitrary sample points X_i and X_j is taken as the Gaussian exponential correlation function

$$R(X_i, X_j) = e^{-\sum_{k=1}^n \theta_k |X_i^k - X_j^k|^{\gamma_k}},$$

where n is the dimension of the input vector X . X_i^k and X_j^k denote the k th elements of the design vectors X_i and X_j respectively. The parameters of the correlation function $\theta_k > 0$ and $0 < \gamma_k < 2$ for $k = 1, \dots, n$ must be tuned to find the setting, which provides the maximum likelihood of the estimator. Note that as the distance between two designs X_i and X_j grows, the correlation function tends to go to zero. In the other extreme case, as the distance between X_i and X_j gets smaller, the correlation function tends to go one. As given in [22], the Kriging estimator to predict the response a new design at X is

$$\tilde{f}(X, \beta_0) = \beta_0 + r^\top \mathcal{R}^{-1} [Y_s - \beta_0 I], \quad (3)$$

where the vectors Y_s (functional values at sample points) and I are given by

$$Y_s = \begin{bmatrix} Y_1 \\ Y_2 \\ \vdots \\ Y_{n_p} \end{bmatrix} \quad \text{and} \quad I = \begin{bmatrix} 1 \\ 1 \\ \vdots \\ 1 \end{bmatrix}.$$

The $n_s \times n_s$ matrix \mathcal{R} , on the other hand, is called as the correlation matrix. It is given by

$$\mathcal{R} = \begin{bmatrix} R(X_1, X_1) & R(X_1, X_2) & \dots & R(X_1, X_{n_s}) \\ R(X_2, X_1) & R(X_2, X_2) & \dots & R(X_2, X_{n_s}) \\ \vdots & \vdots & \ddots & \vdots \\ R(X_{n_s}, X_1) & R(X_{n_s}, X_2) & \dots & R(X_{n_s}, X_{n_s}) \end{bmatrix}.$$

Note that all the diagonal elements of \mathcal{R} are unity since $R(X_i, X_i) = e^0 = 1$, $\forall i \in \{1, \dots, n_s\}$. Furthermore, \mathcal{R} is symmetric since $R(X_i, X_j) = R(X_j, X_i)$, $\forall i, j \in \{1, \dots, n_s\}$.

The vector r in Eq. 3 is a measure of how a new sample at the input X correlates with the initial sample points. It given as

$$r = \begin{bmatrix} R(X_0, X) \\ R(X_1, X) \\ \vdots \\ R(X_{n_s}, X) \end{bmatrix}.$$

The trend function for the ordinary Kriging β_0 can be found by taking the least square estimate. It is given by

$$\beta_0 = [I^\top \mathcal{R}^{-1} I]^{-1} [I^\top \mathcal{R}^{-1} Y_s].$$

A very useful feature of the Kriging method is that the theory provides the mean squared error, which can be taken into account while choosing new sample points. The variance of the Kriging estimator at an untried point X is given as

$$s^2 = \sigma^2 \left[1 - r^\top \mathcal{R}^{-1} r + \frac{(r^\top \mathcal{R}^{-1} I - 1)^2}{I^\top \mathcal{R}^{-1} I} \right], \quad (4)$$

where σ^2 is the maximum likelihood estimate of the unadjusted variance

$$\sigma^2 = \frac{1}{n} [Y_s - \beta_0 I]^\top \mathcal{R}^{-1} [Y_s - \beta_0 I].$$

Also note that the variance s^2 is an indicator of uncertainty of the Kriging approximation at the new sample

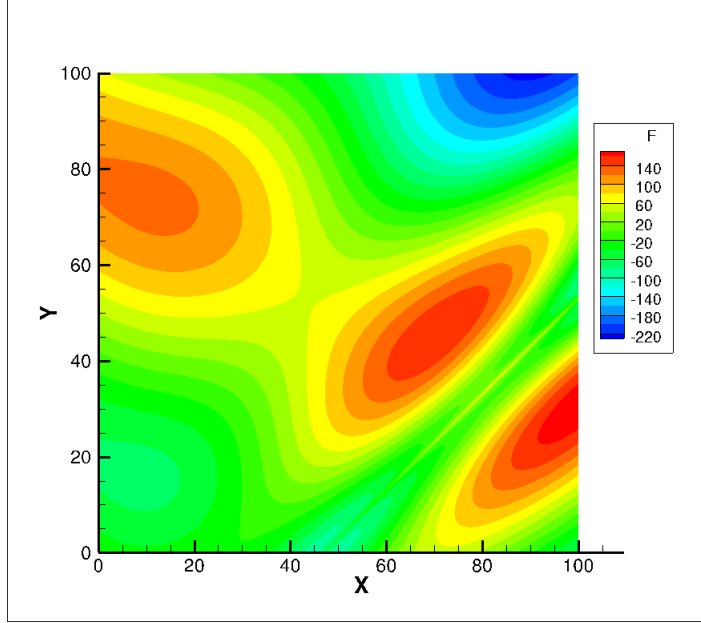


Figure 2: The Eggholder function $f(x, y) = -(y + 47) \sin(\sqrt{|x/2 + y + 47|}) - x \sin(\sqrt{|x - (y + 47)|})$

point X . Higher values of it indicate that the response surface given by the Kriging estimator is likely to deviate from the true response surface. In general, the quality of the Kriging estimator depends on three factors:

- The selection of parameters of the correlation function θ_k and γ_k , $k = 1, \dots, n$.
- The number of samples used to construct the Kriging estimator: n_s .
- The sampling strategy used to choose the initial samples.

The most common approach used to select the parameters of the correlation function is to pick up the values, which maximize a suitable likelihood function. Since we assume that the error term is a Gaussian process, it is appropriate to use the Gaussian log-likelihood function

$$\ell(\theta, \gamma) = -\frac{n_s}{2} (\ln(2\pi) + 1) - \frac{n_s}{2} s^2 - \frac{1}{2} \ln(\det \mathcal{R}).$$

Therefore, the parameters of the correlation function are given from the solution of the optimization problem

$$\max_{\theta, \gamma} \ell(\theta, \gamma), \quad (5)$$

which can be solved efficiently by an EA based global search method.

The second issue, which plays an important role in the quality of the Kriging estimator, is the number of samples used to construct the surrogate model. In Figure 2, the contour plot of the Eggholder function is shown for $0 < x_1 < 100$ and $0 < x_2 < 100$. The Eggholder function is a classical function used to test global optimization algorithms since it is highly non-linear with multiple extrema. In Figures 3 and 4, the response surfaces obtained from the Kriging estimators using 50 and 100 random samples are shown. On the right hand side of each figure, contours of s^2 are also plotted showing the uncertainty of the surrogate model in the sampling domain. One can easily see that, the surrogate model obtained from 50 samples has high amount of uncertainty at some locations and is not capable of reproducing the minimum at the right top corner. Obviously, using 100 samples solves this problem but at the expense of doubling the computational time required for the sampling.

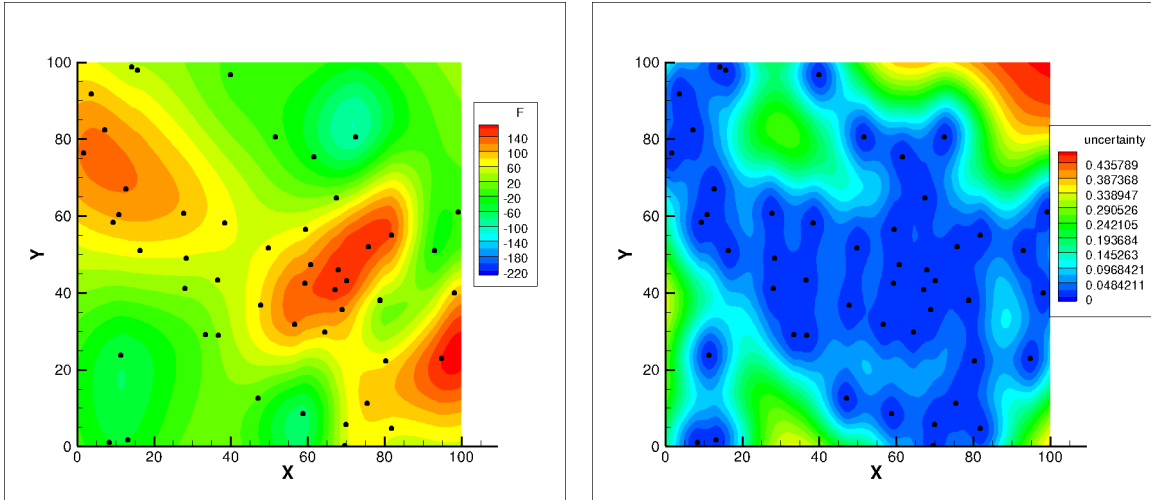


Figure 3: Response surface obtained by the Kriging method using 50 random samples for the Eggholder function

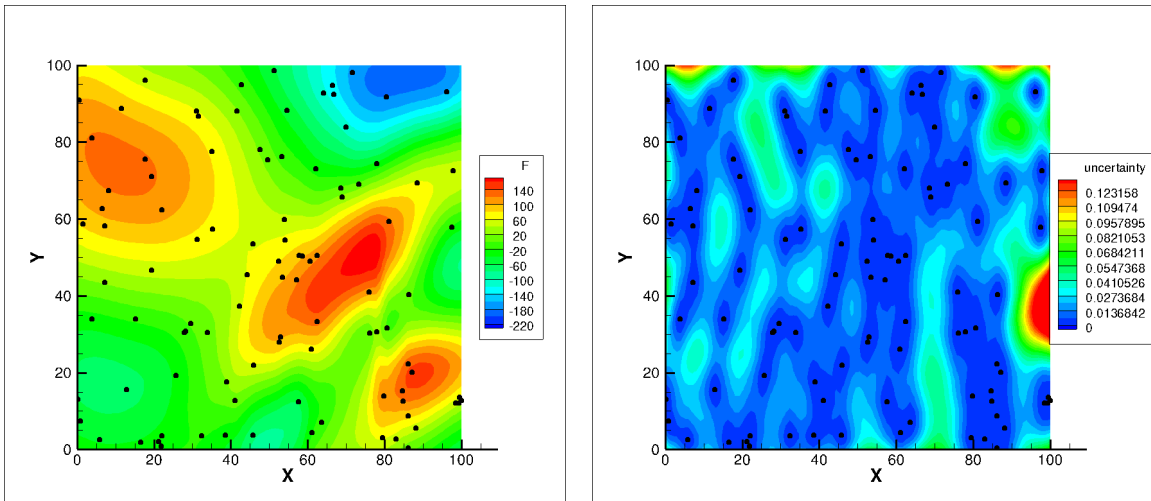


Figure 4: Response surface obtained by the Kriging method using 100 random samples for the Eggholder function

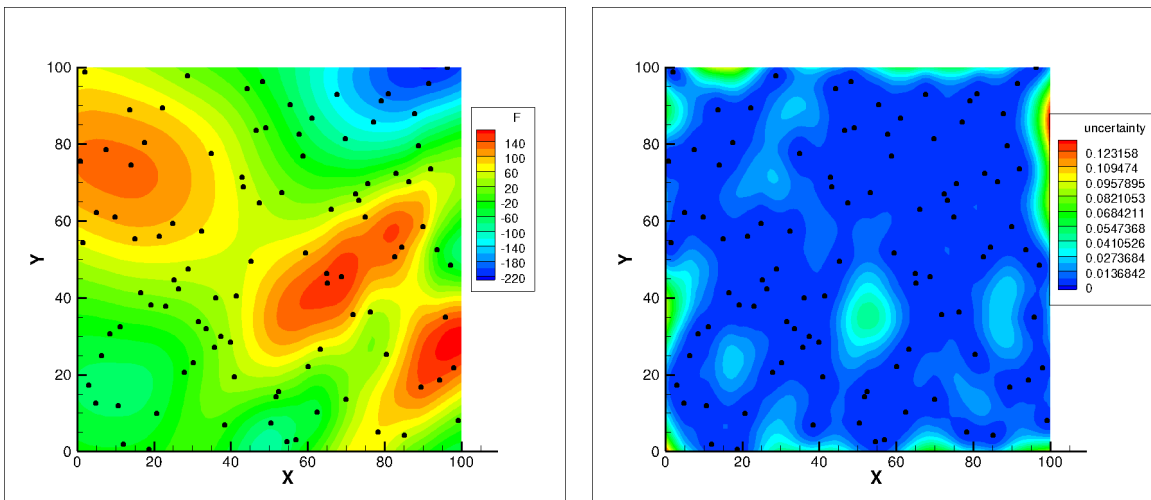


Figure 5: Response surface obtained by the Kriging method using 100 samples (LHS) for the Eggholder function

Another important point affecting the quality of the surrogate model is the distribution of samples used to construct the estimator. In general, it is hard to decide the optimal sampling strategy without having a priori knowledge on the problem. The easiest strategy is of course using uniform or random sampling. For some problems, however, using Latin Hypercube Sampling (LHS) might be more advantageous. As an example, in Figure 5, the response surface obtained from the Kriging estimator using 100 samples chosen by the LHS method is shown. Compared to the results, obtained by 100 random sample points, it can be observed that LHS method leads to better results and less uncertainty of the response surface.

Once the surrogate model based on Kriging method is constructed, an EA based algorithm is used to search the global optimal using a set of box constraints imposed on the design parameters. The lower and upper limits for the box constraints, which generally depend on the results obtained from the numerical simulations, are specified by the user. If the number of samples obtained in the initial data acquisition phase is not adequate, the surrogate model may be inaccurate and the value provided by the global search may not be the real global optimum. An efficient way to explore a more accurate response surface is the Expected Improvement (EI) method, which has been proposed by Mockus et al. [23]. The key idea behind the EI approach is to take into account both the predicted value given by the surrogate model and the uncertainty of that predicted value while deciding the locations of the additional sample points. By evaluating a value of expected improvement, the EI approach provides the most promising new samples that can be added to the existing data. In this way, the surrogate model becomes more and more accurate as additional data points are included. For the minimization of a scalar-valued function J , the improvement function is given by

$$I(X) = \max(J^* - \tilde{J}(X), 0),$$

where J^* is the minimum of the initial data set and $\tilde{J}(X)$ is the predicted value of the objective function by the surrogate model for the given design point X . The Expected Improvement value at a design X is given by

$$E(I(X)) = (J^* - \tilde{J}(X))\Phi\left(\frac{(J^* - \tilde{J}(X))}{s}\right) + s\phi\left(\frac{(J^* - \tilde{J}(X))}{s}\right),$$

where Φ and ϕ are the normal cumulative distribution function (CDF) and the normal probability density function (PDF) respectively. The variable s is the root mean square error of the surrogate model given by the Kriging method and it represents the uncertainty at of the predicted objective function a design point X . As an example, the EI distribution obtained from the Kriging estimator using 100 sample points is shown in Figure 6.

We can summarize the most important steps in the first level as

- Step 1: CAA simulations are performed at the initial sample points.
- Step 2: Optimization problem given in (5) is solved by the EA to determine the parameters of the correlation function, which maximizes the log-likelihood function.
- Step 3: New sample point, which has the maximum value of EI, is determined by the EA based on the Kriging surrogate model.
- Step 4: New sample point is added to the existing data set and procedure is repeated from the Step 2 until a certain number of iterations is exceeded.

3.2 Gradient-Based Optimization Using Discrete Adjoint Approach

Since we use a high dimensional design space for the gradient search in the second level, the most appropriate way to evaluate the gradient vector is to employ an adjoint CAA solver. In this way, we ensure that the computational cost of the local optimization using the gradient search remains bounded irrespective of the number of liner patches used in optimization. In the following, we shortly introduce the unsteady discrete adjoint methodology used to develop the CAA adjoint solver used in the present work. For simplicity of the derivation, we consider the minimization of a scalar objective function, which is a function of the state vector over a time interval $[0, T]$

$$J = J(Y(T)),$$

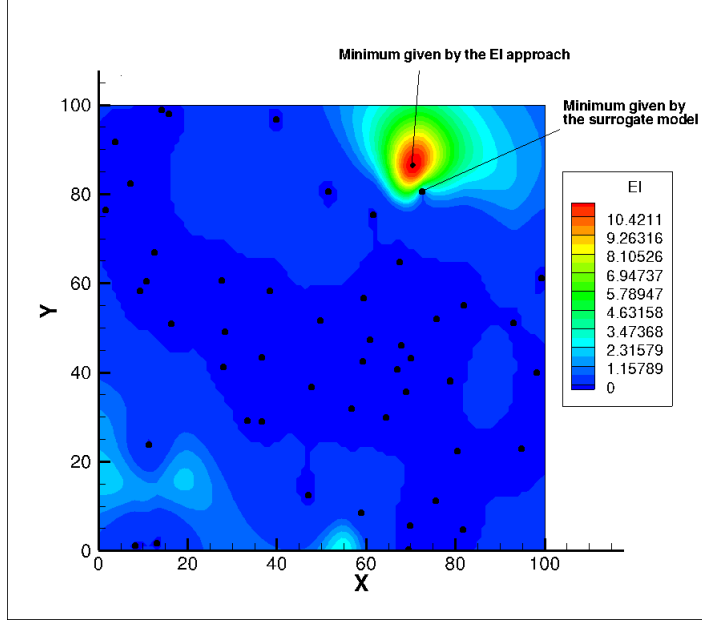


Figure 6: The distribution of the Expected Improvement (EI) for the Eggholder example

where $Y(T)$ is the value of the state vector at the time $t = T$. Although the objective function depends explicitly only on the final solution, it also depends on the design vector implicitly. The design vector $X \in \mathbb{R}^n$, which in our case is the EHR model parameters $\epsilon, \beta, R_f, m_f$ and T_l in each liner patch, influences the state solution during the forward-in-time integration of the CAA simulation via the liner boundary condition given by the acoustic impedance model (Eq. 2). Assuming that we have discrete state solutions $Y_0, Y_1, Y_2, \dots, Y_N$ in N time-steps over the time interval $[0, T]$, the true dependency between the objective function J and the design vector X can be written as

$$J = J(Y_N) \quad \text{such that} \quad Y_{k+1} = G(Y_k, X), \quad k = 0, 1, \dots, N-1,$$

where G is a discrete mapping of the state vector into itself. In the CAA context, the discrete mapping G in the above equation corresponds to the set of operations performed within a single time iteration of the LEE solver and it includes all the intermediate Runge-Kutta stages of the temporal LDDRK scheme. In other words, assuming that all other boundary conditions other than the acoustic impedance at the lined section are fixed, the forward trajectory of the dynamical system imposed by the LEE equations is determined only by the initial value of the state vector Y_0 and the design vector X . In short, the optimization problem can be written with the state constraint as

$$\min_X J(Y_N) \quad \text{such that} \quad Y_{k+1} = G(Y_k, X), \quad k = 0, 1, \dots, N-1.$$

For the gradient search optimization we require the total derivative of J with respect to X . If the objective function J is differentiated with respect to the design parameter vector X , we get.

$$\frac{dJ}{dX} = \frac{dJ}{dY_N} \frac{dY_N}{dX}.$$

On the other hand differentiating the discrete mappings $Y_{k+1} = G(Y_k, X)$, $k = 0, 1, \dots, N-1$ with respect to design X , we get the expressions

$$\begin{aligned}
\frac{dY_1}{dX} &= \frac{\partial G(Y_0, X)}{\partial X} + \frac{\partial G(Y_0, X)}{\partial Y_0} \frac{dY_0}{dX} = \frac{\partial G(Y_0, X)}{\partial X} \\
\frac{dY_2}{dX} &= \frac{\partial G(Y_1, X)}{\partial X} + \frac{\partial G(Y_1, X)}{\partial Y_1} \frac{dY_1}{dX} = \frac{\partial G(Y_1, X)}{\partial X} + \frac{\partial G(Y_1, X)}{\partial Y_1} \frac{\partial G(Y_0, X)}{\partial X} \\
\frac{dY_3}{dX} &= \frac{\partial G(Y_2, X)}{\partial X} + \frac{\partial G(Y_2, X)}{\partial Y_2} \frac{dY_2}{dX} = \frac{\partial G(Y_2, X)}{\partial X} + \frac{\partial G(Y_2, X)}{\partial Y_2} \frac{\partial G(Y_1, X)}{\partial X} \\
&+ \frac{\partial G(Y_2, X)}{\partial Y_2} \frac{\partial G(Y_1, X)}{\partial Y_1} \frac{\partial G(Y_0, X)}{\partial X} \\
&\vdots \\
\frac{dY_N}{dX} &= \frac{\partial G(Y_{N-1}, X)}{\partial X} + \frac{\partial G(Y_{N-1}, X)}{\partial Y_{N-1}} \frac{dY_{N-1}}{dX} = \frac{\partial G(Y_{N-1}, X)}{\partial X} \\
&+ \frac{\partial G(Y_{N-1}, X)}{\partial Y_{N-1}} \frac{\partial G(Y_{N-2}, X)}{\partial X} \\
&+ \frac{\partial G(Y_{N-1}, X)}{\partial Y_{N-1}} \frac{\partial G(Y_{N-2}, X)}{\partial Y_{N-2}} \frac{\partial G(Y_{N-3}, X)}{\partial X} + \dots \\
&+ \frac{\partial G(Y_{N-1}, X)}{\partial Y_{N-1}} \frac{\partial G(Y_{N-2}, X)}{\partial Y_{N-2}} \frac{\partial G(Y_{N-3}, X)}{\partial Y_{N-3}} \dots \frac{\partial G(Y_0, X)}{\partial X}.
\end{aligned}$$

Using the expression for the derivative dY_N/dX from the above equation, the total derivative dJ/dX can be reformulated as

$$\begin{aligned}
\frac{dJ}{dX} &= \frac{\partial J}{\partial X} + \frac{\partial J}{\partial Y_N} \frac{\partial G(Y_{N-1}, X)}{\partial X} + \frac{\partial J}{\partial Y_N} \frac{\partial G(Y_{N-1}, X)}{\partial Y_{N-1}} \frac{\partial G(Y_{N-2}, X)}{\partial X} \\
&+ \frac{\partial J}{\partial Y_N} \frac{\partial G(Y_{N-1}, X)}{\partial Y_{N-1}} \frac{\partial G(Y_{N-2}, X)}{\partial Y_{N-2}} \frac{\partial G(Y_{N-3}, X)}{\partial X} + \dots \\
&+ \frac{\partial J}{\partial Y_N} \frac{\partial G(Y_{N-1}, X)}{\partial Y_{N-1}} \frac{\partial G(Y_{N-2}, X)}{\partial Y_{N-2}} \frac{\partial G(Y_{N-3}, X)}{\partial Y_{N-3}} \dots \frac{\partial G(Y_0, X)}{\partial X}. \tag{6}
\end{aligned}$$

Multiplying the above expression with a weight vector (column vector) $\dot{X} \in \mathbb{R}^n$, we get the so-called direct discrete sensitivity equation

$$\begin{aligned}
\frac{dJ}{dX} \dot{X} &= \frac{\partial J}{\partial X} \dot{X} + \frac{\partial J}{\partial Y_N} \frac{\partial G(Y_{N-1}, X)}{\partial X} \dot{X} + \frac{\partial J}{\partial Y_N} \frac{\partial G(Y_{N-1}, X)}{\partial Y_{N-1}} \frac{\partial G(Y_{N-2}, X)}{\partial X} \dot{X} \\
&+ \frac{\partial J}{\partial Y_N} \frac{\partial G(Y_{N-1}, X)}{\partial Y_{N-1}} \frac{\partial G(Y_{N-2}, X)}{\partial Y_{N-2}} \frac{\partial G(Y_{N-3}, X)}{\partial X} \dot{X} + \dots \\
&+ \frac{\partial J}{\partial Y_N} \frac{\partial G(Y_{N-1}, X)}{\partial Y_{N-1}} \frac{\partial G(Y_{N-2}, X)}{\partial Y_{N-2}} \frac{\partial G(Y_{N-3}, X)}{\partial Y_{N-3}} \dots \frac{\partial G(Y_0, X)}{\partial X} \dot{X},
\end{aligned}$$

which gives the directional derivative of J in the direction of \dot{X} . The exact implementation of the above equation can be realized by differentiating the complete simulation chain by the forward mode of AD. In CAA context, this corresponds differentiating the complete CAA solver with the AD tool. This process generates a "tangent-linear" CAA solver, which is an exact implementation of the operations given in above. Note that using the tangent-linear solver only a single component of the gradient can be evaluated. Therefore, for large n , evaluating the gradient vector with a tangent-linear solver is infeasible.

On the other hand, if we take the transpose of the both sides in Eq. 6, we obtain

$$\begin{aligned} \frac{dJ^\top}{dX} &= \frac{\partial J^\top}{\partial X} + \frac{\partial G(Y_{N-1}, X)^\top}{\partial X} \frac{\partial J^\top}{\partial Y_N} + \frac{\partial G(Y_{N-2}, X)^\top}{\partial X} \frac{\partial G(Y_{N-1}, X)^\top}{\partial Y_{N-1}} \frac{\partial J^\top}{\partial Y_N} \\ &+ \frac{\partial G(Y_{N-3}, X)^\top}{\partial X} \frac{\partial G(Y_{N-2}, X)^\top}{\partial Y_{N-2}} \frac{\partial G(Y_{N-1}, X)^\top}{\partial Y_{N-1}} \frac{\partial J^\top}{\partial Y_N} + \dots \\ &+ \frac{\partial G(Y_0, X)^\top}{\partial X} \dots \frac{\partial G(Y_{N-3}, X)^\top}{\partial Y_{N-3}} \frac{\partial G(Y_{N-2}, X)^\top}{\partial Y_{N-2}} \frac{\partial G(Y_{N-1}, X)^\top}{\partial Y_{N-1}} \frac{\partial J^\top}{\partial Y_N}. \end{aligned}$$

The above equation can be rearranged as

$$\frac{dJ^\top}{dX} = \frac{\partial J^\top}{\partial X} + \sum_{i=N}^1 \frac{\partial G(Y_{i-1}, X)^\top}{\partial X} \phi_i, \quad (7)$$

where the vectors ϕ_i , $i = N, N-1, \dots, 1$ are given by the recursion

$$\phi_N = \frac{\partial J^\top}{\partial Y_N} \quad \text{and} \quad \phi_i = \frac{\partial G(Y_i, X)^\top}{\partial Y_i} \phi_{i+1}, \quad i = N-1, N-2, \dots, 1. \quad (8)$$

In this way, we obtained the adjoint sensitivity equation that evaluates the gradient vector at one stroke. Similar to a tangent-linear solver, the adjoint solver that exactly implements the solution procedure given in Eqs. (7) and (8) can be generated automatically by applying AD techniques on the source code of the underlying CAA solver. In this way, all parts of the CAA solver such as spatial and temporal schemes, boundary conditions etc. are differentiated exactly and the discrete adjoint CAA solver inherits all the features of the underlying CAA solver. In the present work, the Algorithmic Differentiation process of the underlying CAA solver has been accomplished by using the source transformation tool Tapenade [24].

Note that the computations in Eq. (8) require that the values of the state vector Y must be available in reverse order. In other words, the values of state vector in the order Y_N, Y_{N-1}, \dots, Y_0 must be available during the adjoint computation. However, due to the iterative nature of the CAA solver, the state vector is updated after every iteration during the forward-in-time integration of. As a result, the values of the state vector are no more available for the adjoint computation. This problem can be solved by saving these values in each iteration, but this approach becomes unfeasible for large scale applications with many time iterations as the memory requirements may quickly exceed the available memory. To reduce memory requirements, checkpointing strategies are employed, in which the flow solutions are stored only at selective time iterations. These values are then used to recompute the intermediate states that are not stored. In the present work, a two-level checkpointing algorithm has been employed [25]. This approach generates a checkpointing schedule such that both RAM and disk checkpoints are used in an optimal way to offer the best compromise between run-time and memory requirements.

We can summarize the most important steps in the second level as

- Step 1: The high-dimensional design vector is initialized using the best design from the first level.
- Step 2: The gradient vector is evaluated by the CAA adjoint solver.
- Step 3: The vector of design parameters is updated according to BFGS method.
- Step 4: At the new design, a CAA simulation is performed to measure the improvement. If the stopping criteria is not fulfilled, the procedure is repeated starting from the Step 2.

4 Liner Optimization for the Turbofan By-pass Duct Configuration

In order to show the applicability and efficiency of the two-level method, a design optimization study on a generic by-pass duct of a turbofan engine with bifurcations is performed. The objective function used

in the optimization study is the sound power, according to the definition of Morfey [26]. In Figure 7, the by-pass duct geometry including bifurcations is shown. The surfaces, in which the sound power integration is carried out are displayed in blue. For the present study, we integrate the sound power at the second surface close to the outlet. The duct length is 1.84m. At the inlet, the inner diameter is 0.5m and the outer diameter is 0.84m. At the outlet, the inner diameter is 0.64m and the outer diameter is 1.0m. The CAA aspects of configuration are discussed by Schönwald et al [27] in detail. The by-pass duct configuration is particularly suitable to test the suggested optimization approach since it features all the important aspects of sound propagation in turbofan by-pass ducts as well as the interaction of sound waves with the hard walls and the liner. The computational grid, which is used for CAA and adjoint computations, has a multi-block structure realized by applying the Chimera (overset) technique. Therefore, the entire computational domain has a nearly equidistant and locally orthogonal O-type grid that forms the host grid. For the bifurcations, which is treated by the overset grid, body-fitted O-type grids are used. The computational grid consists of approximately 10^6 grid points, distributed over 68 computational blocks. In Figure 8, the computational grid is shown on the left. In the right, the overset grid (red) for the bifurcations is shown at the cut interface between the overset grid and the host grid. The largest grid spacing is around 6.5 mm, which corresponds to approximately 11.5 point per wave. For the forward-in-time integration, we take 3360 time iterations with the CFL number is set to 0.5. The computations are carried out using 64 cores. As far as the acoustic source is considered, two acoustic modes at $f = 1700$ Hz and $f = 47000$ Hz are excited. As the boundary conditions, a non-reflecting modal acoustic source at the inlet and a non-reflective PML boundary at the outlet are used. The mean flow quantities required in the CAA and adjoint computations are calculated by RANS simulation using the commercial flow solver STARCCM+. Since an unstructured grid is used for the flow simulation, the simulation results are interpolated from the CFD grid onto the structured CAA grid.

For the EA based global search in the first level, we use a parameterization with a single liner patch. As a result, the liner parameters are not allowed to vary spatially at the lined section of duct at this stage of the optimization. The lined wall sections at the inner and outer duct surfaces are shown in Figure 9. For the initial data acquisition phase, which is required to construct the surrogate model, CAA simulations at 100 different design points are carried out. Using the Kriging surrogate model, which is constructed using the initial data, a global optimization using the EA algorithm is performed. Totally, 20 additional samples, which have the maximum expected improvement value in each iteration, are added into the data. In the second level, the number of liner patches is increased to 80 with totally 400 design parameters. The liner parameters are initialized using the best design from the first level. As the gradient search algorithm, BFGS algorithm is employed. The gradient information, which is required by the BFGS update is evaluated using the discrete adjoint CAA solver. In Figure 11, the sensitivity maps of different liner parameters calculated at the beginning of the second level are shown. These adjoint sensitivities at each CV face are integrated by the adjoint solver to evaluate the design sensitivities at each liner patch. As the stopping criteria, the descent tolerance of the objective function in successive iterations is used. The optimization process is terminated after performing 5 iterations after 5 adjoint and 5 function evaluations. In Table 1, the values of the objective function achieved in each level of the optimization process are tabulated. The sound power without the liner (hard wall case) is calculated to be 6.981 W. Among the 100 samples in the initial data acquisition phase, the best liner design has the sound power 0.223 W, which means that 96 % reduction was already achieved compared to the hard wall case. After the global optimization in the first level, the sound power was further decreased to 0.130 W, which means that 41 % reduction compared to the best liner design in the initial data set was achieved. Increasing the number of liner parameters in the second level brought another 26 % reduction compared to the first level optimal solution. The sound power at this best design was calculated to be 0.096 W. In Figures 12, the optimal distribution of the EHR model parameters achieved at the end of second level are presented.

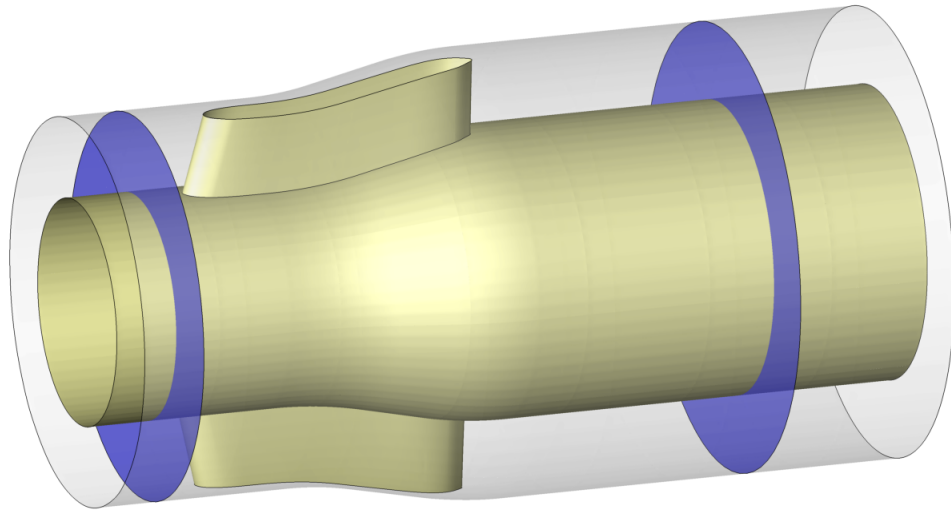


Figure 7: The by-pass duct configuration with bifurcations and power integration surfaces

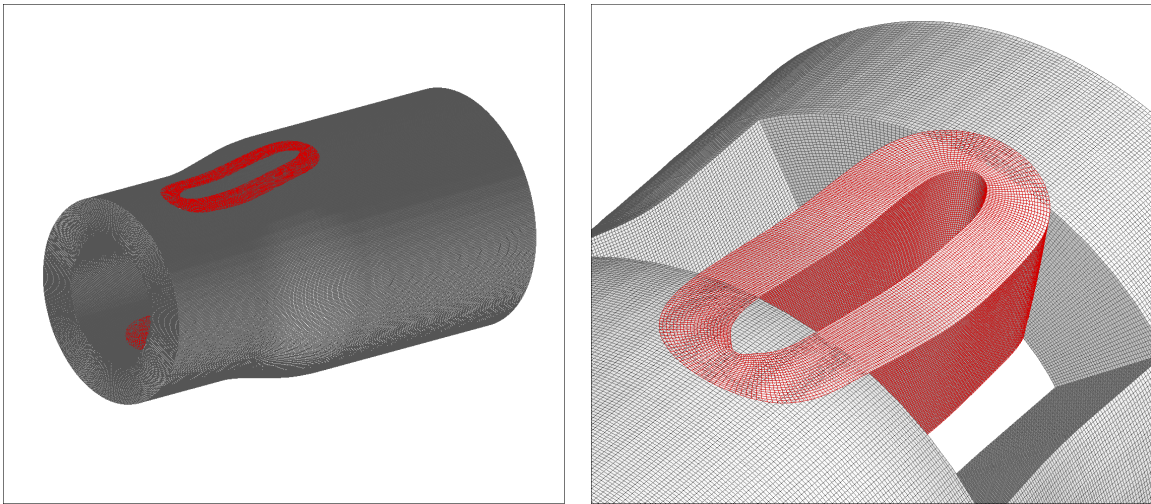


Figure 8: Computational grid used for the by-pass duct configuration used in the CAA and adjoint simulations (left) and overset grid for the bifurcations shown at a cut interface (right)

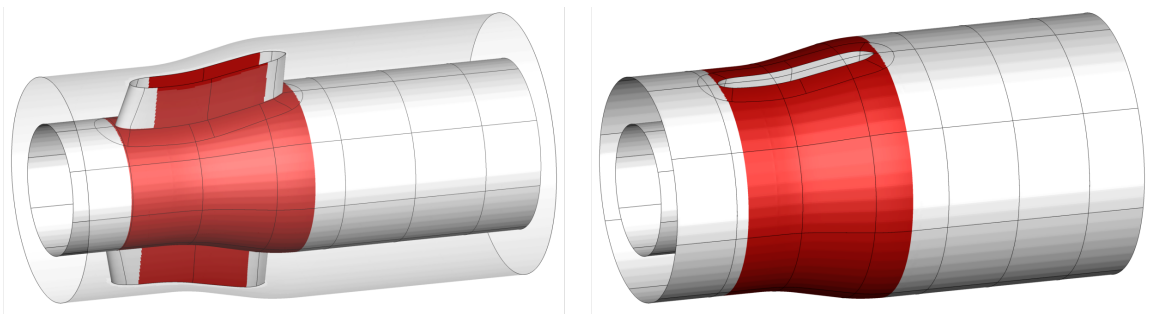


Figure 9: Lined wall section for the single patch liner configuration at the inner duct surface (left) and at the outer duct surface (right)

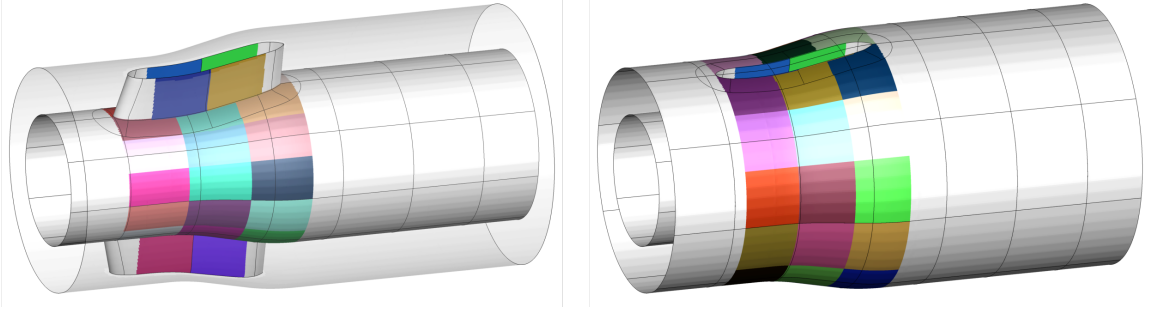


Figure 10: Lined wall section for the configuration with 80 liner patches at the inner duct surface (left) and at the outer duct surface (right)

Configuration	Sound power (W)	% Reduction
Hard wall case	6.981	-
Best design in the initial sampling	0.223	96
Optimal single patch liner (first level)	0.130	41
Optimal spatially variable liner with 80 patches (second level)	0.096	26

Table 1: Comparison of the sound power for the initial liner setting, global liner optimization with single liner patch and two-level optimization using 80 liner patches at the second level.

5 Conclusions

In this paper, we presented a two-level optimization approach for the design optimization of acoustic liners. The two-level method is realized by combining an EA based global optimization strategy with a gradient search method using an unsteady discrete adjoint CAA solver. The global optimization in the first level is carried out using a surrogate model based on Kriging approach. The discrete adjoint solver, used in the second level, was developed by applying Algorithmic Differentiation (AD) techniques to the source code of the underlying CAA solver. The adjoint CAA solver retains the full functionality of the underlying CAA solver. The efficiency of the suggested two-level method was then demonstrated by finding the optimal liner distribution of a turbofan by-pass duct.

Acknowledgements

The authors gratefully acknowledge the computing time granted by the Allianz für Hochleistungsrechnen Rheinland-Pfalz (AHRP), Germany.

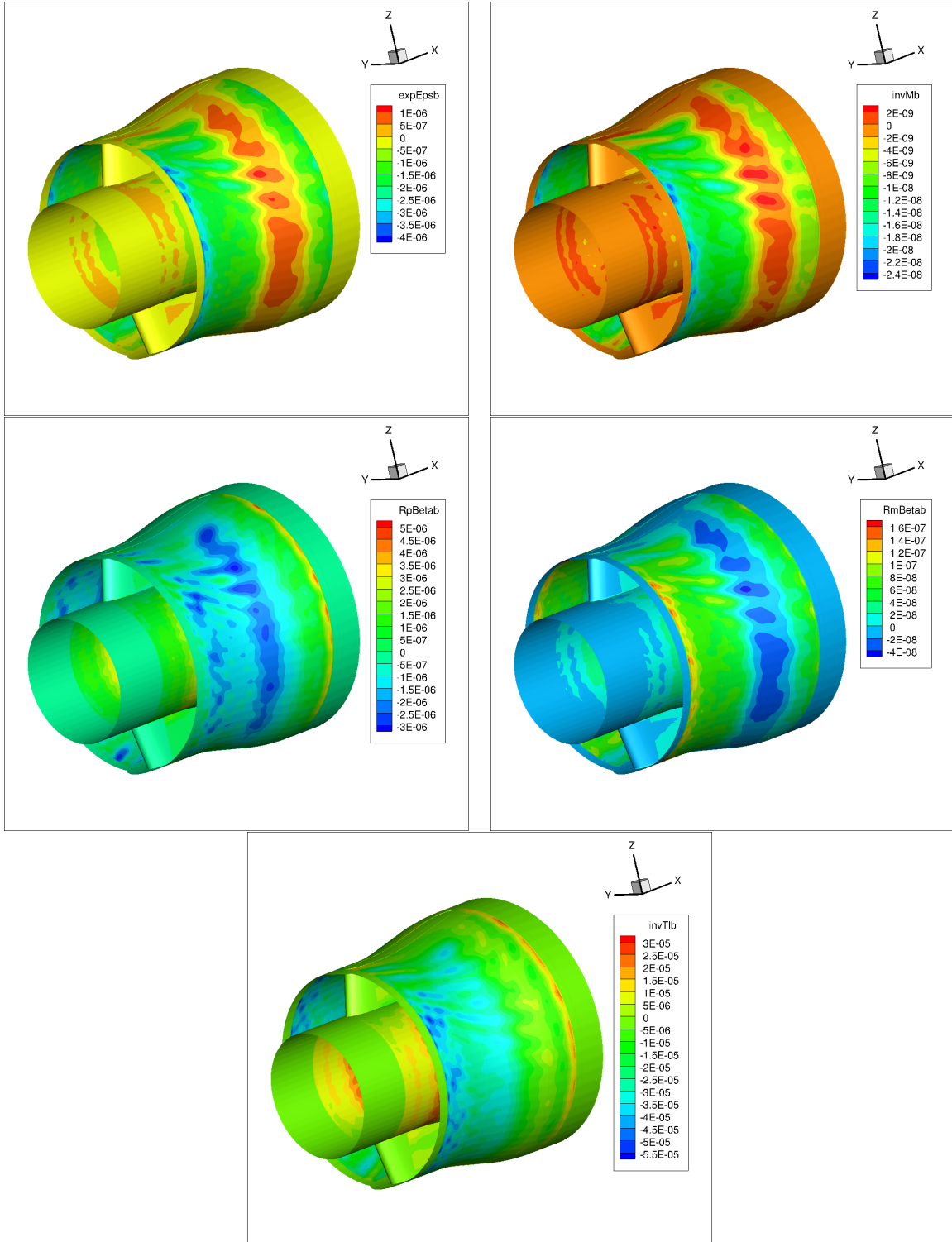


Figure 11: Sensitivity maps of liner parameters at the beginning of gradient search in the second level. Top left: $dJ/d(e^{-\epsilon})$. Top right: $dJ/d(1/m_f)$. Middle left: $dJ/d(R_f + \beta)$. Middle right: $dJ/d(R_f - \beta)$. Bottom: $dJ/d(1/T_l)$.

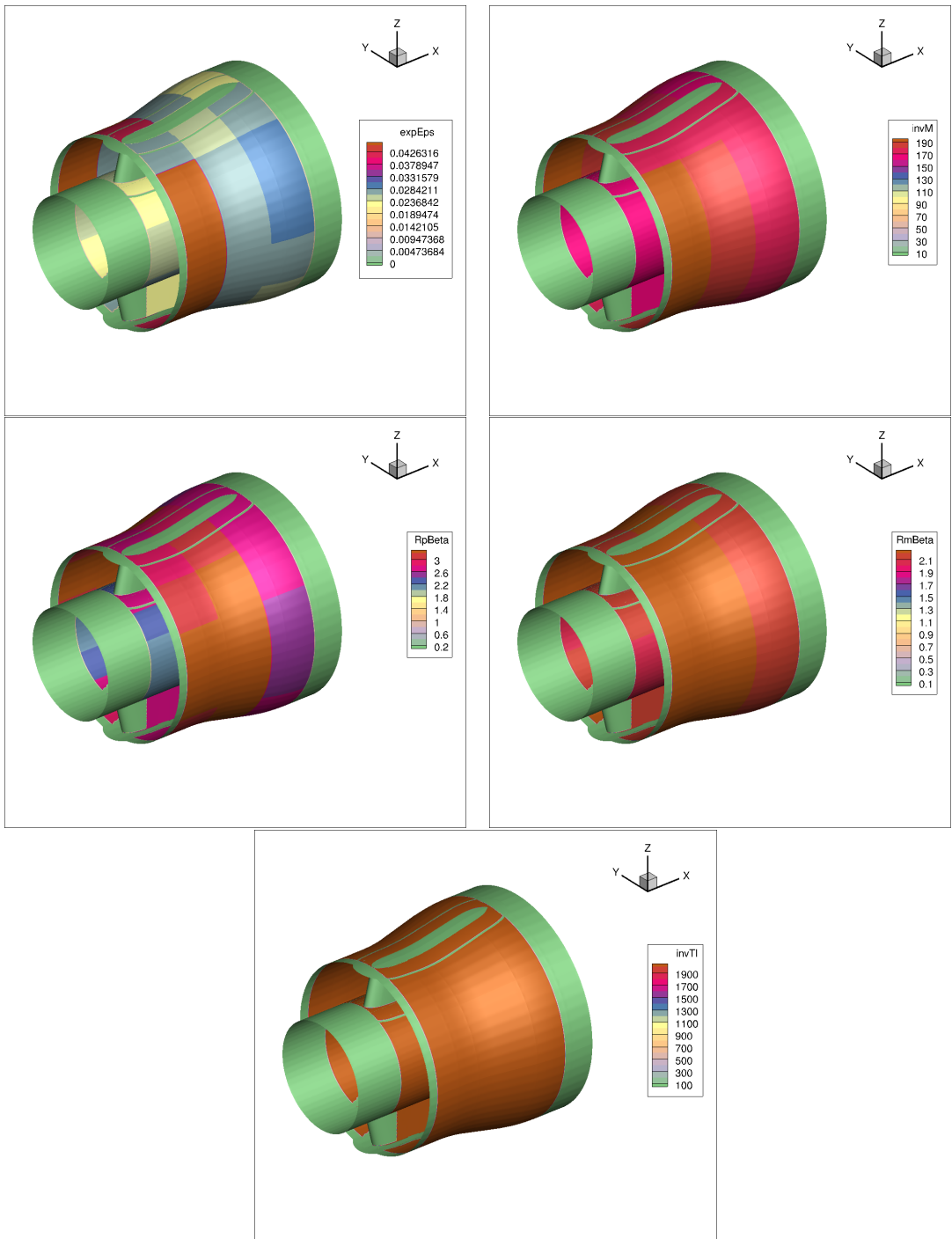


Figure 12: Optimal lined wall section for the configuration with 80 liner patches: Top left : Optimal distribution of $e^{-\epsilon}$. Top right: Optimal distribution of $1/m_f$. Middle left: Optimal distribution of $(R_f + \beta)$. Middle right: Optimal distribution of $(R_f - \beta)$. Bottom: Optimal distribution of $1/T_l$.

References

- [1] A. Jameson, L. Martinelli, and N. A. Pierce. Optimum aerodynamic design using the Navier-Stokes equations. *Theoretical and Computational Fluid Dynamics*, 10(1):213–237, 1998.
- [2] E. J. Nielsen and W. K. Anderson. Aerodynamic design optimisation on unstructured meshes using the Navier-Stokes equations. *AIAA Journal*, 37(11):185–191, 1999.
- [3] A. Griewank and A. Walther. *Evaluating derivatives: Principles and techniques of Algorithmic Differentiation*. SIAM, 2008.
- [4] A. Nemili, E. Özkaya, N. R. Gauger, F. Kramer, T. Höll, and F. Thiele. Optimal design of active flow control for a complex high-lift configuration. Technical report, 2014.
- [5] B. Y. Zhou, N. R. Gauger, S. R. Koh, and M. Meinke W. Schröder. On the adjoint-based control of trailing-edge turbulence and noise minimization via porous material. AIAA Paper 2015-2530, 2015.
- [6] D. Quagliarella and A. Della Cioppa. Genetic algorithms applied to the aerodynamic design of transonic airfoils. *Journal of Aircraft*, 32(4):889–891, 1995.
- [7] A. Oyama, S. Obayashi, and K. Nakahashi. Transonic wing optimization using genetic algorithm. AIAA Paper 97-1854, 1997.
- [8] Z.-H. Han, K.-S. Zhang, W.-P. Song, and Z.-D. Qiao. Optimization of active flow control over an airfoil using a surrogate-management framework. *Journal of Aircraft*, 47:603–612, 2010.
- [9] W. Yamazaki, M. P. Rumpfkeil, and D. J. Mavriplis. Design optimization utilizing Gradient/Hessian enhanced surrogate model. AIAA Paper 2010-4363, 2010.
- [10] S. K. Jeong, M. Murayama, and K. Yamamoto. Efficient optimization design method using kriging model. *J. Aircraft*, 42(2):413–420, 2005.
- [11] J. W. Yim, B. J. Lee, and C. Kim. Exploring multi-stage shape optimization strategy of multi-body geometries using Kriging-based model and adjoint method. *Computers & Fluids*, 68:71 – 87, 2012.
- [12] C. K. W. Tam and C. Webb. Dispersion-relation-preserving finite difference schemes for computational aeroacoustics. *Journal of Computational Physics*, 107(8):262–281, 1993.
- [13] F. Q. Hu, M. Y. Hussaini, and J. Manthey. Low-dissipation and low-dispersion Runge-Kutta schemes of computational acoustics. *Journal of Computational Physics*, 124(1):177–191, 1996.
- [14] D. Stanescu and W. G. Habashi. 2N-storage low-dissipation and low-dispersion Runge-Kutta schemes for computational aeroacoustics. *Journal of Computational Physics*, 143(2):674–681, 1998.
- [15] C. K. W. Tam. Advances in numerical boundary conditions for computational aeroacoustics. *Journal of Computational Acoustics*, 6(2):377–402, 1998.
- [16] F. Q. Hu. A stable perfectly matched layer for Linearized Euler Equations in unsplit physical variables. *Journal of Computational Physics*, 173(2):455–480, 2001.
- [17] S. W. Rienstra. Impedance models in time domain including the extended Helmholtz resonator model. AIAA Paper 2006-2686, 2006.
- [18] U. Ingard. Influence of fluid motion past a plane boundary on sound reflection, absorption, and transmission. *J. Acoust. Soc. Am.*, 31:1035–1036, 1959.
- [19] M. Myers. On the acoustic boundary condition in the presence of flow. *J. Sound Vib.*, 71:429–434, 1980.
- [20] D.G. Krige. Statistical approach to some basic mine valuations problems on the witwatersrand. *Journal of the Chemical, Metallurgical and Mining Engineering Society of South Africa*, 52(6):119–139, 1952.
- [21] D. R. Jones, M. Schonlau, and W. J. Welch. Efficient global optimization of expensive black-box functions. *Journal of Global Optimization*, 13:455–492, 1998.
- [22] J. Sacks, W. J. Welch, T. J. Mitchell, and H. P. Wynn. Design and analysis of computer experiments. *Statistical Science*, 4:409–423, 1989.
- [23] J. Mockus, V. Tiesis, and A. Zilinskas. The application of Bayesian methods for seeking the extremum. *Towards Global Optimization*, 2:117–129, 1978.
- [24] L. Hascoet and V. Pascual. The Tapenade Automatic Differentiation tool: Principles, model, and specification. *ACM Trans. Math. Softw.*, 39(3):20:1–20:43, 2013.
- [25] E. Özkaya, J. Abdel Hay, N. R. Gauger, and F. Thiele. Development of an adjoint CAA solver for design optimization of acoustic liners. AIAA Paper 2016-2778, 2016.
- [26] C.L. Morfey. Acoustic energy in non-uniform flows. *Towards Global Optimization*, 14:159–170, 1971.
- [27] N. Schönwald, L. Panek, C. Richter, and F. Thiele. Mode propagation in bifurcated bypass ducts: Application oriented simulation approach. AIAA Paper 2010-3895, 2010.